Electronic Supplementary Material (ESI) for Green Chemistry.

Electronic Supplementary Information

Understanding factors controlling depolymerization and polymerization in catalytic degradation of model lignin by versatile peroxidase

Jijiao Zeng, Matthew J. L. Mills, Blake A. Simmons, Michael S. Kent, Kenneth L. Sale

I. Experimental Data

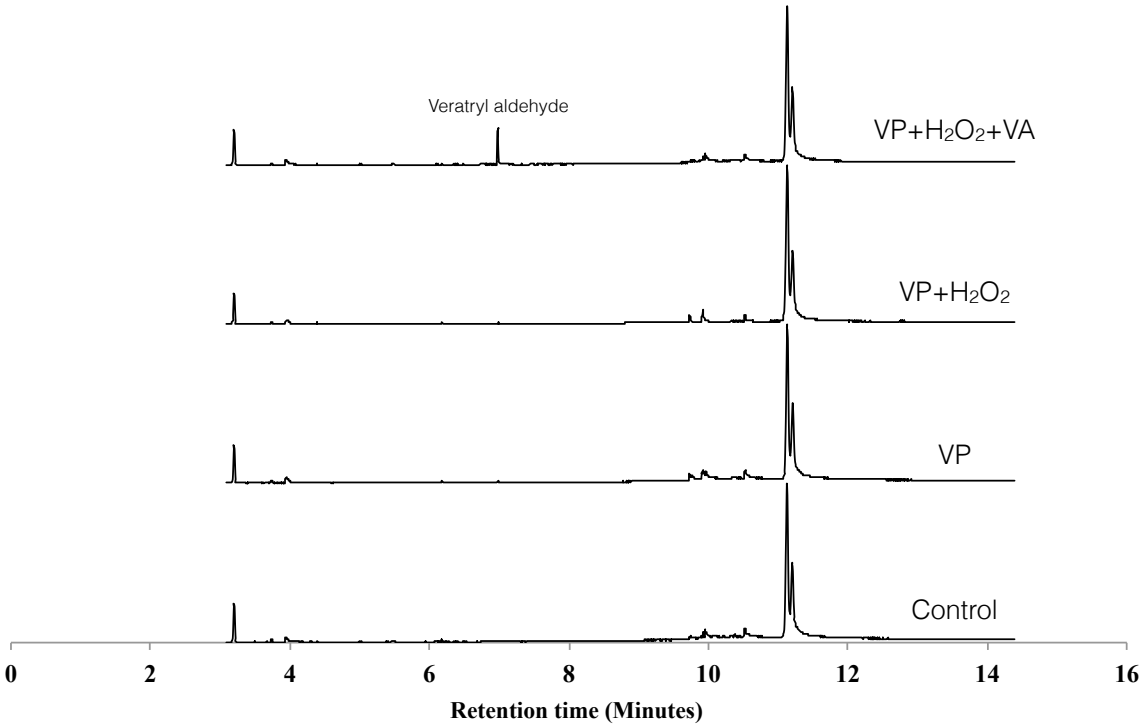

Figure S1 - GC/MS spectra of the products of the VP_*Bad*-catalyzed reaction of the non-phenolic substrate *V*-O-4 in the presence/absence of H_2O_2 and VA at pH 4.5. The control contains *V*-O-4, water and sodium malonate buffer. Additional species are marked on each line.

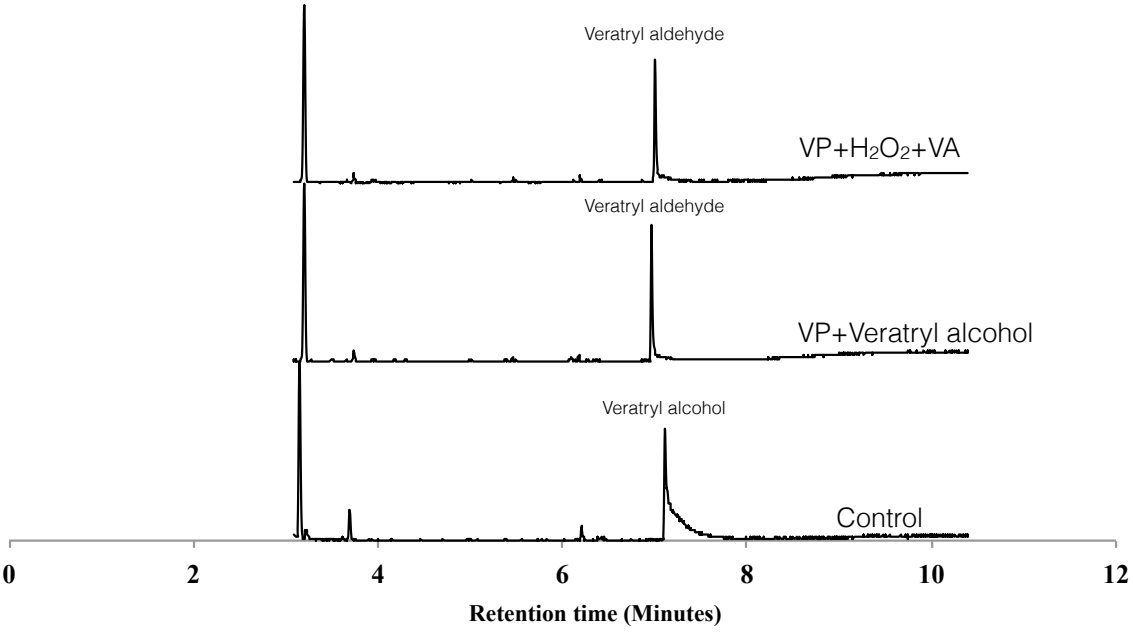

Figure S2 - GC/MS spectra of the products of the VP_*Bad*-catalyzed reaction of VA in the presence/absence of H_2O_2 at pH 4.5.

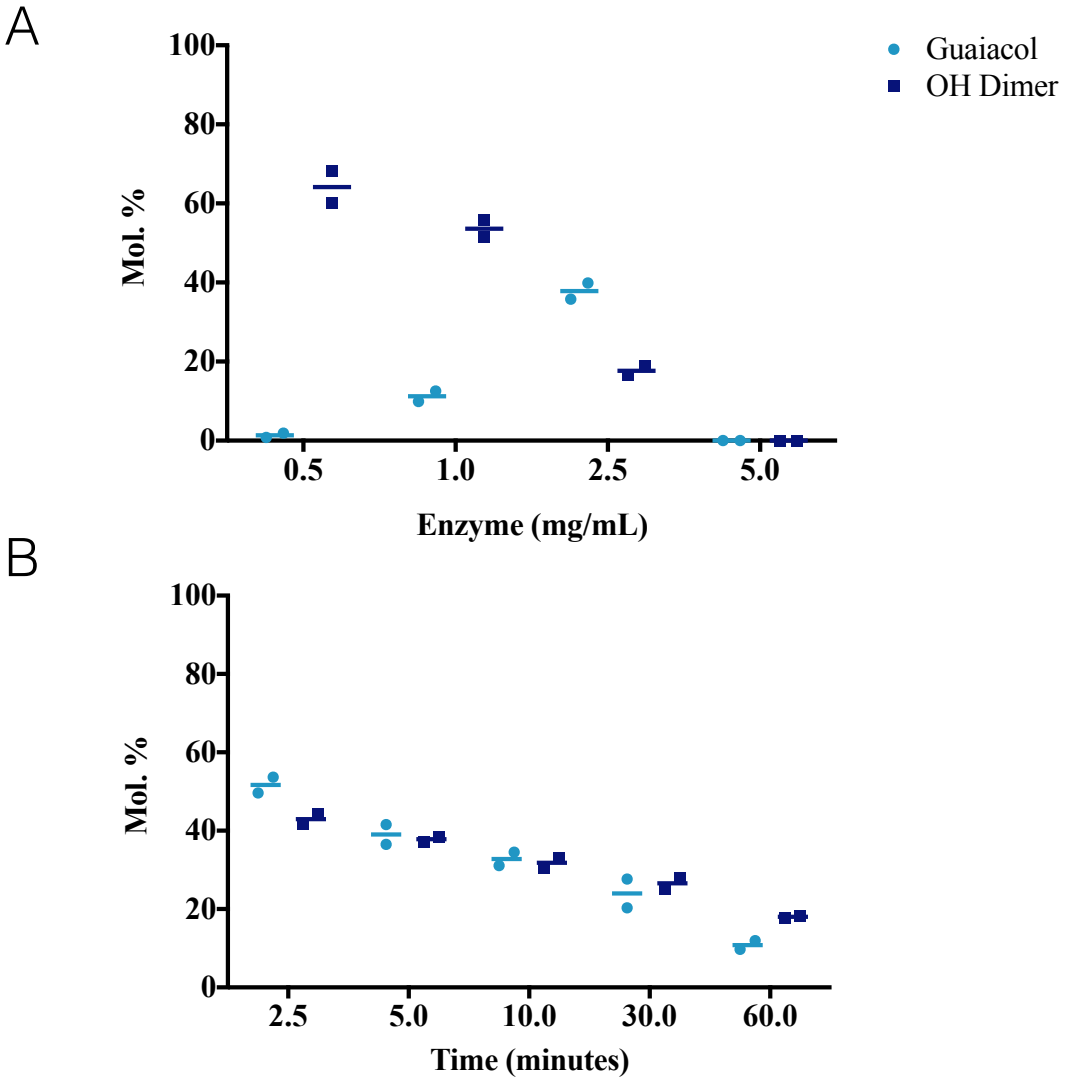

Figure S3 - The effect of A) enzyme concentration and B) reaction time on the conversion of the phenolic *G*-O-4 dimer to products at pH 4.5 with 10 mM H_2O_2.

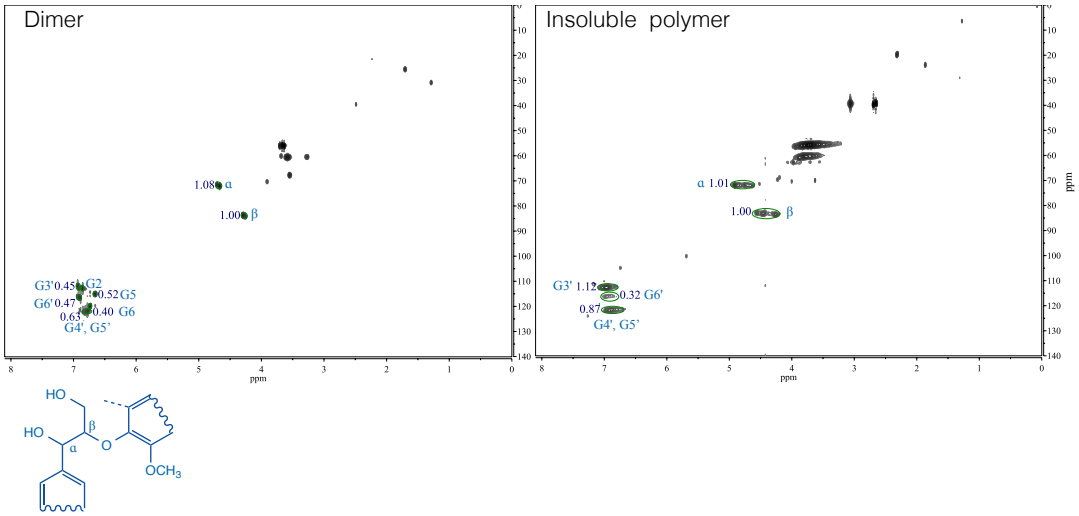

Figure S4 – The global HSQC spectra of dimer and insoluble polymer. Integrals for the aromatic region and aliphatic region integrals are listed. The integral ratio between α-OH and *β*-H is approximately 1 for both samples which suggests that the alpha-OH is not involved in the polymerization reaction. The ratio $I_{G6'}/I_{\beta}$ is smaller in the spectrum of the polymer compared with its value in the spectrum of the dimer. That could be partially due to the increased T2 relaxation time of the polymer during the NMR analysis. Also, the contour of G6 is not evident in the HSQC spectra for the polymer, but based on the spin density calculated for the activated substrates it is unlikely that G6' and G6 are involved in the reaction. The reason for the absence of G6 in the spectrum for the polymer is unclear. It may have shifted such that it lies underneath the peak for G 5' and G 4'.

II. Computational Research

Introduction

This supplementary document describes in detail the methods used to obtain the theoretical results discussed in the main text, and is also intended to establish their relevance to the systems that have been studied experimentally. The explicit atomistic investigation of these systems is far too computationally expensive to be tractable, particularly as certain of the properties that must be evaluated are inherently quantum mechanical, meaning that standard force field- and molecular mechanics-based methods (which would allow simulations over long time scales) are not applicable. Herein, a density functional theory and continuum solvation modeling approach (see Methods and Materials) is taken to evaluate free energies associated with chemical changes in aqueous solution. The reacting system is treated as a set of half-cell equations, and redox potentials are determined from the free energies of formation. Relative conformational energies, redox potentials and resonance (quantified by atomically partitioned spin densities) are sufficient to explain the experimental results described in the main text.

In particular, the redox potential calculations explain the experimental observations that the versatile peroxidase from *Bjerkandera adusta* (VP_*Bad*) exhibits no activity on a non-phenolic lignin dimer, yet displays activity on two different phenolic dimers and on veratryl alcohol (VA), a common radical mediator for lignin-degrading enzymes. The spin density calculations also assist in understanding both the tendency towards depolymerization and polymerization of the oxidized phenolic dimers, and the particular linkages observed in polymerization products. The experimental system consists of the VP_*Bad* enzyme in aqueous solution with sodium malonate buffer. In addition, the various conditions tested include the presence/absence of VA, manganese, hydrogen peroxide and the three different model lignin dimer compounds.

The VP Enzyme

Versatile peroxidase enzymes exhibit two activities, catalyzing oxidation of low redox potential substrates by producing diffusible Mn^{3+} species from Mn^{2+} ions, and oxidation of high redox potential substrates via a tryptophan site on their outer surface[1]. The complete redox cycle is detailed in Fig. 1A. A substrate-oxidation pathway via a neutral radical, where the tryptophan residue is deprotonated at the nitrogen atom, has been experimentally observed via EPR[2, 3]. After the radical is formed by reaction of the enzyme's heme cofactor with H_2O_2, the Trp residue can remove a proton and electron from substrates to produce corresponding neutral radicals. Direct computation of the oxidation potential of this site is particularly challenging, but bounds can be set on its value using experimental data and calculations of the ability of VP_*Bad* to oxidize different substrates.

Veratryl Alcohol Species

Experimental data suggest that VP_*Bad* can catalyze oxidation of VA (see main text Fig. 2). However, as the data presented in Fig. S2 shows, oxidation of VA (but not the lignin-model dimers) is possible without the oxidant H_2O_2 present, which (see Fig. 1) is required for activation of the heme center. Therefore, either a secondary oxidant (potentially molecular oxygen) is able to cycle the active site, or an impurity is present in the enzyme (i.e. the purchased enzyme is not only VP_*Bad* and may contain, for example, another enzyme with LiP activity that can leverage a secondary oxidant). A third possibility is the existence of another, as yet unknown, VA-specific and H_2O_2-independent functionality in VP_*Bad.* Future work will clarify this observation; the following information on the oxidation potentials of VA is of interest independent of the results. The steps from initial VA radical formation through conversion to the aldehyde product are shown in Fig. S4. Each arrow of the diagram corresponds to a chemical half-reaction for which the free energy change is to be evaluated. Initial removal of an electron (the leftmost arrow) forms the corresponding radical cation, which can further become either of two possible neutral radical isomers depending on the position at which a single proton is removed. Alternatively (and supported by experiment[2] as the correct enzymatically-catalyzed pathway in VP_*Bad*) the proton and electron may be removed in a single step. Both possibilities are considered herein so that

conclusions about the enzyme can be drawn independently from previously reported experiments.

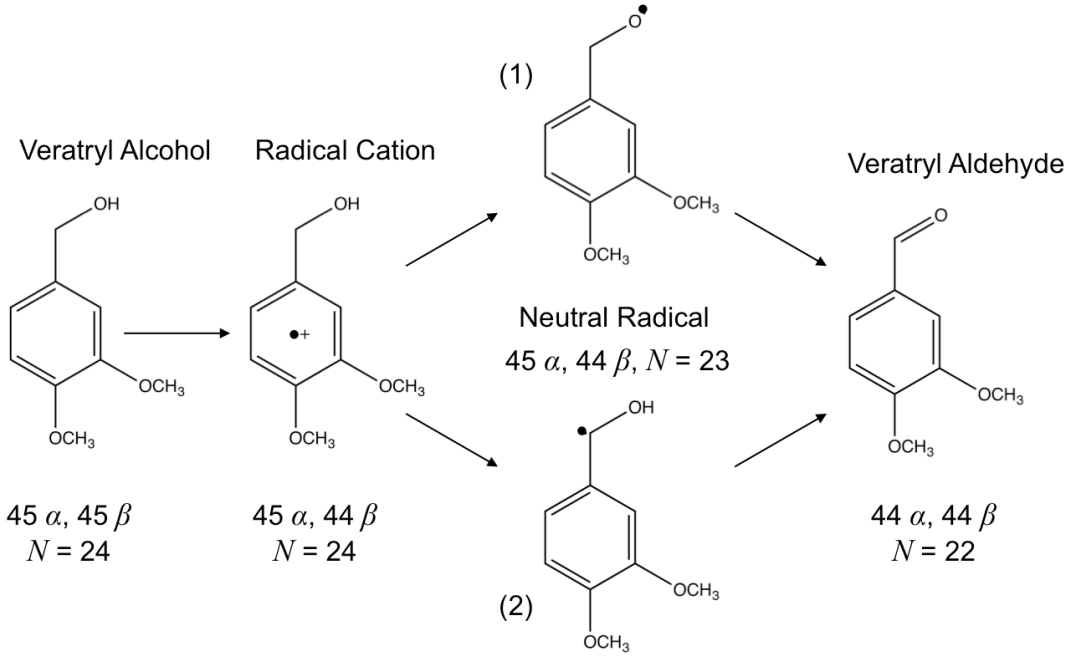

Figure S5 – Pathway for conversion of veratryl alcohol to veratryl aldehyde. The number of α and β-spin electrons for each species is given, along with N, the number of nuclei. The two possible neutral radicals formed by deprotonation at different positions are labeled (1) and (2).

Model Substrates

Three model lignin dimer substrates were studied experimentally in this work, one non-phenolic (veratrylglycerol-*β*-guaiacyl ether - *V*-O-4) and two phenolic (syringyl and guaiacylglycerol-*β*-guaiacyl ether – *S*-O-4 and *G*-O-4 respectively). The chemical structures and names are shown in Fig. 1B.

Diagrams analogous to the VA diagram of Fig. S4 can be drawn for each of these substrates (see Fig. 2B). The process is similar, in that a radical cation can be formed from each substrate. Each of these high-energy species can then react to form a neutral radical with loss of one proton - the possible deprotonation positions (α, β, and γ of the glycerol moiety and the aryl 4-OH position) are labeled in Fig. 1B - and the neutral radical may also be produced directly from the substrate. Once formed, radical generation is then followed by either depolymerization (through bond-breaking) or repolymerization (through bond-forming) reactions.

Experiments show that *V*-O-4 does not react in the presence of any oxidant produced by the enzyme (Fig. S1), while *G*-O-4 and *S*-O-4 do react with the enzyme (Figs. 2A and 5D). The experimental results also show that position 5 is critical for the chemical path followed by the phenolic *G*-O-4 and *S*-O-4 species (see Fig. 5). If occupied by a methoxy group (as in *S*-O-4), the radical species

depolymerizes to form the observed monomeric product, guaiacol (Fig. 5E). Conversely, if the group at position 5 is a hydrogen atom (as in *G*-O-4), the dimer will polymerize (Figs. 5A and 5B) to form an insoluble, high molecular weight product with a distribution of linkage positions, the majority of which are between the 4 and 5' positions (Fig. 5C).

Methods

Half-cell Equations and their Corresponding Reduction Potentials

Results for the study in question are most clearly presented in terms of the redox potentials of half-cell equations, allowing conclusions to be made based on free energies. By convention, a half-cell equation is written with electrons e^- and protons H^+ on the left-hand side, as a reduction.

$$aA + bB + n[\mathrm{e}^-] + h[\mathrm{H}^+] \rightarrow cC + dD$$

A, B and C, D are the chemical species consumed and created respectively in the reaction; a, b, c, d, n and h are stoichiometric coefficients. In order to discuss the redox behavior of the various components of the system, it is necessary to enumerate their various possible half-cell equations and subsequently compute the corresponding potentials.

The standard potential, E_0, for a particular half-cell equation is related to the corresponding Gibbs free energy change, ΔG (which can be computed from first principles as described below).

$$E_0 = -\Delta G/nF \qquad (1)$$

The free energy change is measured in J mol^{-1}, n is the number of electrons transferred (and is the same quantity appearing in the half-cell equation) and F is Faraday's constant, $F = eN_A = 96485.32289$ C mol^{-1}, wherein e is the elementary charge of the electron and N_A is Avogadro's constant. The resulting values of E_0 are measured in Volts (J/C). The energy conversion factor from the more commonly used kcal mol^{-1} to J mol^{-1} is 4184.

The potential associated with a process described by a half-cell equation measures the tendency of the involved chemical species to acquire electrons (be 'reduced') or lose electrons (be 'oxidized'). More positive potentials (corresponding to more negative free energy changes) indicate a greater affinity of the left-hand side species for electrons, and that species C and D are more stable. Negative potentials (positive free energy changes) indicate that the right hand species have a tendency to lose electrons, i.e. species A and B are more stable with protons and electrons removed. Finally, a pair of half-equations can be combined by reversing one, adding the species on each side, and summing the potentials. By this procedure the feasibility of various reactions in solution can be determined.

Free Energy Changes in Solution

As noted above, a route to computing free energy changes for reactions is required to evaluate the potentials of half-equations. Values of ΔG for use in Eqn. 1 are computed herein by approximating the configuration space of the system as a limited set of minimum energy (on the potential energy surface) conformations, allowing properties to be evaluated as Boltzmann weighted averages. Experiments produce observables corresponding to the average values of a given property A, thus it is necessary to compute the mean value of A over the system's phase space.

$$\langle A \rangle = \sum_{i=0}^{N-1} A_i \, P(A_i)$$

Here i runs over each of the N states of the system. From statistical mechanics, the probability, $P(A_i)$, of finding the system in the particular state i that produces the property value A_i is known to be proportional to the energy E_i and is given by $P(A_i) = \exp[-E_i/k_B T]$ (where T is temperature). The mean of A can then be written in terms of properties and energy values.

$$\langle A \rangle = \frac{1}{Z} \sum_{i=0}^{N-1} A_i \, e^{-E_i/k_B T} \qquad (2)$$

This equation introduces the normalization constant, Z (the partition function), which is required to ensure that the sum over all probabilities is equal to unity.

$$Z = \sum_{i=0}^{N-1} e^{-E_i/k_B T}$$

In discussion of the conformational distributions of chemical species, it is often useful to be able to assign a quantitative importance to a single conformation. Given the form of the observed value of A in Eqn. 2, each conformation contributes a factor of $e^{-E_i/k_B T}/Z$ of its property value to the mean. Thus we can rank the importance of a given conformation, i, to a reported value by converting this factor to a percentage contribution.

$$X_i = 100 \frac{e^{-E_i/k_B T}}{Z} \qquad (3)$$

This property can be thought of as the percentage population of a given state, i.e. the probability that any randomly drawn single molecule will be in the conformation indexed by i. The values of X_i over a conformational distribution sum to 100 % by definition.

To evaluate the free energies, the radical species are assumed to be present in solution. This allows the free energies of individual molecules (small enough to be treated quantum mechanically) to be evaluated, including the solvation energy of removed protons. The free energies of reaction for the processes related to

lignin decomposition can be computed without describing either the enzyme (a significantly more involved and difficult problem) or the details of reaction mechanisms. This limits this study to determination of free energies of reaction only and means that kinetic effects are not addressed. For radical formation processes, there is often no free energy barrier to reaction and this assumption was carried throughout the rest of this work.

Even for small systems (such as VA) it is not possible to enumerate all of the possible conformations necessary for the exact evaluation of Eqn. 2, so the common approximation that at the relevant temperature the system spends most of its time near its potential energy minima was adopted. As such, observations that would be made over the complete conformational space can be approximated well with a much smaller set of conformations. This holds when a few conformations exist that are significantly lower in energy than the remainder, as then most of the terms in Eqn. 2 are close to zero. This also allows the elimination of any conformation whose energy contributes less than some threshold (e.g. 10%) to the average, which allows for computational resources to be focused on higher-level quantum methods. The approximation also holds when the property in question is not highly dependent on conformation.

Quantifying Resonance with Atomic Spin Densities

The concept of resonance is often employed to qualitatively evaluate the relative stabilities of different radical isomers. It is also possible to infer reactivity patterns from probability distributions of the unpaired electron in different locations within the radicals. A molecule can be represented by a set of structures where the unpaired electron is in different positions, with the implication that delocalization of the electrons is responsible for lowering the total energy of the system. The concept can be quantified by the examination of the electronic spin density of chemical species, wherein a more delocalized spin density corresponds to systems for which a larger number of resonance forms can be drawn.

The spin density is a 3D scalar function defined in real space, and quantifies the difference in density between α and β spin electrons at a point in space, $\mathbf{r}$.

$$\rho_s(\mathbf{r}) = \rho_\alpha(\mathbf{r}) - \rho_\beta(\mathbf{r})$$

Reasoning based on spin densities is made more straightforward (compared to inspection of a 3D surface) by defining *atomic* values of spin density. As noted in the main text, this is possible via the theory of Atoms in Molecules, which allows the definition of atomic properties as volume integrals over spatial regions that can be associated with atoms. This is a parameter-free method that allows first principles calculations of atomically partitioned values of any quantum mechanical operator.

$$A_{\Omega_i} = \int_{\Omega_i} A(\mathbf{r})$$

The integration is carried out numerically over the complex 3D shape Ω, termed the atomic basin, which is uniquely determined by the theory. By determining a representative set of conformations and calculating the atomic spin densities of

each, Eqn. 2 can be used to determine a properly averaged spin density for a given atom within a molecule.

Computational Details

Quantum chemical results were obtained, and conformational searches performed, as stated in the main text (Materials and Methods). The representative set of unique conformations for each molecule was filtered based on both energy and geometry. Any pair of conformations equal in energy to 1.0×10^{-6} Hartrees (the SCF convergence criterion) were considered identical. This approach removes conformations that differ only by methyl or hydroxyl group rotations. Pairs of conformations with energies differing by larger than the energy threshold were compared by computation of their root mean square deviation (RMSD) in Cartesian space.

$$\mathrm{RMSD}_{AB} = \sqrt{\frac{1}{N}\sum_{n=0}^{N-1}\sum_{i=0}^{2}\left(\alpha_{n,A}^{i} - \alpha_{n,B}^{i}\right)^{2}}$$

Here A and B denote the 2 conformations of N atoms, and $\alpha = \{x, y, z\}$ is the set of coordinates for atom *n*. This quantifies the difference in the 3D coordinates. Conformations with RMSD values below 0.01 Å were considered identical.

For VA and derived species, all conformations located by the search were used in the subsequent analysis. For the larger substrate molecules (i.e. those shown in Fig. 1B), the results were filtered to achieve a feasible computational load by retaining only those conformations that represent the 99th percentile of the most energetically feasible states of the conformational ensemble. This approach reduced the required number of computations for each species by between 76 and 94 % (details are provided in Table S2).

Results and Discussion

1 – Veratryl Alcohol

The results of the conformational analysis of the various relevant VA-derived species are collected in Table S1. This table gives the total number of unique gas phase conformations located and the energy range occupied for each species. The range of free energies of each conformation is also provided, and in the rightmost column the percentage populations (see Eqn. 3) of each conformation are displayed. Each species is essentially fully represented by at least 3 and at most 4 lowest energy (highest probability) conformations.

Chemical Species	Num. Confs.	ΔE	ΔG	% Population X_i
				0 30 60
Veratryl Alcohol	26	5.4	6.5	
Neutral Radical (1)	8	1.1	5.6	
Neutral Radical (2)	13	3.3	3.2	
Radical Cation	13	4.7	5.3	

Table S1 – Details of gas-phase conformational searches for VA-derived species. All energy-range values (the difference between the lowest and highest value obtained) are in kcal mol^{-1}. Distributions of the conformations in aqueous solution are provided, where each dot represents a single located minimum energy conformation on the PES. Many of these are clustered around zero.

The free energies of formation of radicals from VA are shown in Fig. S5 and indicate that each step of the process involves a positive free energy change. It is also evident that the neutral radical formed by loss of a proton from the CH_2 group is much more stable (17 kcal mol^{-1}) than that formed by deprotonation of the OH group. Figure S6 provides a rationale for this observation based on atomic spin densities. Deprotonation of the hydroxyl group results in significantly localized spin density, whereas deprotonation at the carbon atom results in distribution of spin density throughout the molecule. From the values in Fig. S5 the system will preferably follow the lower path depicted in Fig. S4, provided no significant difference in the kinetics of the reaction is present. As a result, the neutral radical with its unpaired electron located on O will not be discussed further.

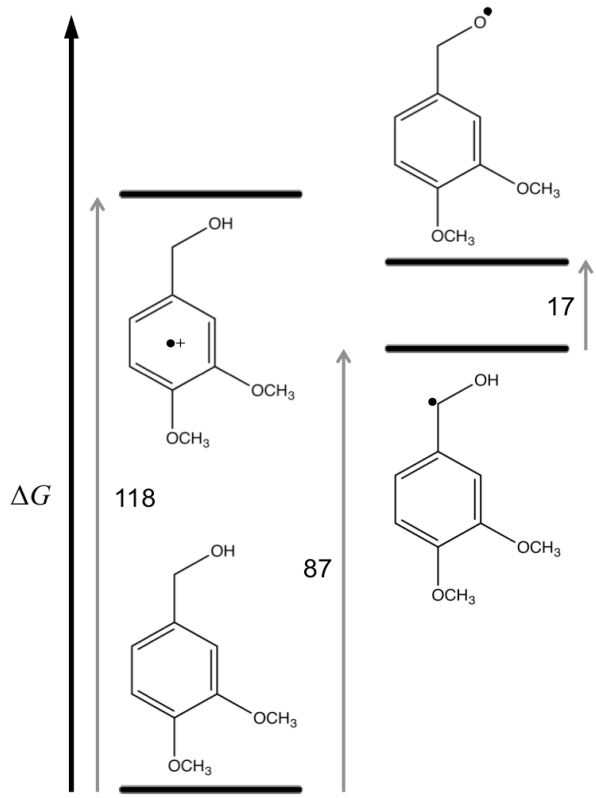

Figure S6– Free energy changes (in kcal mol^{-1}) in aqueous solution connecting each species observed during the veratryl alcohol radicalization process.

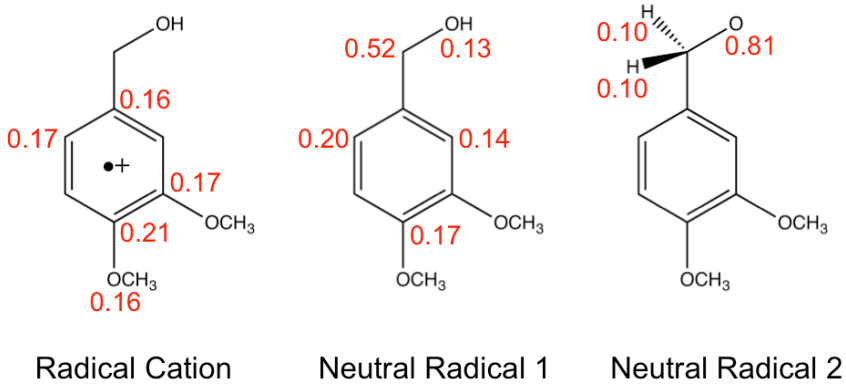

Radical Cation Neutral Radical 1 Neutral Radical 2

Figure S7 – QCT-derived, conformational average (using Eqn. 2) atomic spin density values (in atomic units) for the VA-derived radical species: the radical cation; neutral radical formed by deprotonating at C; and the neutral radical formed by deprotonating at O. Values with magnitude less than 0.1 au are not shown.

The combination of the scheme in Fig. S4 and the free energies reported in Fig. S5 allow enumeration of the appropriate half-cell equations and their corresponding potentials (in Volts), obtained via Eqn. 1. It has not been assumed that the VP_*Bad* enzyme specifically produces the neutral or cationic VA radical in solution, so either of those two processes depicted in Fig. S4 may be enabled by the enzyme.

$$\mathrm{VA}^{\cdot+} + \mathrm{e}^- \rightarrow \mathrm{VA} \quad (E_0 = +5.1)$$

$$\mathrm{VA}^{\cdot} + \mathrm{e}^- + \mathrm{H}^+ \rightarrow \mathrm{VA} \quad (E_0 = +3.8)$$

In either case the oxidation of VA is a highly energetically demanding process. The first possibility produces a much stronger oxidant but constitutes a greater challenge for the enzyme. As VP_*Bad* catalyzes oxidization of VA, the potential associated with the Trp site must have a magnitude of at least 3.8 Volts.

Assuming the radical cation is produced, the simplest process that can occur in solution is recapture of an electron to reform VA. The second alternative corresponds to the second arrow of Fig, S4.

$$\mathrm{VA}^{\cdot} + \mathrm{H}^+ \rightarrow \mathrm{VA}^{\cdot+} \quad (E_0 = +1.3)$$

This corresponds to deprotonation of the radical cation to form the neutral radical. The results suggest that if the enzyme produces the VA radical cation, this species can either oxidize other species (with potential -5.1 V) to reform VA, or be converted to the neutral radical (with potential -1.4 V). The neutral radical species can either reform VA (with potential -3.7 V), creating neutral radicals of other species, or continue along the pathway to form the product. The product of the reaction observed in experiments is veratryl aldehyde, and the lack of any other related product indicates that the neutral radical does not participate in any bond-forming reactions.

2 – Model Lignin Substrates

The exact route from each substrate to its observed products is unknown; therefore, it is initially necessary to consider each possible path. Due to the size of the lignin model dimer molecules, only the conformations constituting the first 99% of the total population of each substrate is carried through in the subsequent analysis. The number of unique minima for each dimer is collected in Table S2.

The large number of unique minima observed for each species is due to the high conformational flexibility of the dimer molecules, which originally inspired the conformational search approach. The similar energy range (10-20 kcal mol^{-1}) observed for all but the *G*-O-4 α–H and β-H is taken to mean that the conformational searches were similarly extensive and that it is unlikely that any low energy minima were missed. Since a small number of lowest energy conformations (between 1 and 23) contribute to 99% of the expected population of each dimer, much of the conformational variation can be safely ignored. The

variation in solvated energies among the 99% (1-6 kcal mol^{-1}) is significantly smaller than the variation of the top 1% in the gas phase.

Species	Unique Confs.	Range ΔE	Num. Confs 99%	Range ΔG	% Population X_i 0 50 100
V-O-4	90 (100)	16.7	6	2.6	
Rad. Cat.	85 (99)	14.8	10	4.7	
γ-OH	70 (94)	16.6	23	5.0	
γ-H	84 (95)	16.5	10	2.4	
α–OH	88 (100)	13.7	15	4.9	
β-H	86 (100)	11.5	26	4.7	
α–H	77 (100)	19.2	2	1.8	
S-O-4	94 (100)	13.3	23	3.9	
Rad. Cat.	92 (99)	18.4	5	5.1	
γ-OH	72 (94)	12.8	19	5.8	
γ-H	88 (89)	10.4	17	5.3	
4-OH	63 (99)	17.7	6	5.9	
α–OH	92 (100)	12.0	10	3.6	
β-H	73 (100)	14.9	4	1.4	
α–H	74 (100)	17.8	3	1.9	
G-O-4	72 (100)	18.9	11	2.2	
Rad. Cat.	95 (100)	18.4	8	3.9	
γ-OH	70 (96)	19.8	12	2.8	
γ-H	69 (92)	13.5	17	4.9	
4-OH	71 (100)	16.6	8	3.0	
α–OH	69 (100)	15.3	5	1.2	
β-H	86 (100)	70.4	7	1.9	
α–H	79 (99)	80.1	1	0.0	

Table S2 – Details of conformational searches of the various model lignin dimer substrates. The number of unique conformations is given (with total completed geometry optimizations out of 100 attempted shown in parentheses) along with the range of gas phase energies of those conformers. The number of conformations needed to retain 99% of the gas phase population is given, along with the conformational distribution and range of free energies of those conformations in aqueous solution. All energies are given in kcal mol^{-1}.

In order to calculate redox potentials for formation of the cationic and neutral radical species it is necessary to compute the free energies accompanying these changes. The free energy of reaction data in aqueous solution relative to each neutral, closed-shell substrate are collected in Table S3 and are plotted in Fig. S7. The aforementioned assumption that these processes are barrierless allows reasoning based on changes in free energies of reaction (or equivalently oxidation potentials) alone.

Consideration of the results in Table S3 and Fig. S7 allows one to dismiss the neutral radicals (Fig. S7, grey lines) formed by deprotonation at γ-OH, γ-H, α–OH and β-H. In comparison to species formed by removing the 4-OH and α–H

protons, these isomers are higher in free energy (by >20 kcal mol^{-1} in general). The resonance concept can again be invoked to understand the relative energetic ordering of the various possible neutral radicals. Deprotonation at α–H results in a species for which at least 2 resonance structures can be drawn, whereas deprotonation at 4-OH allows the unpaired electron to be located at various positions around the phenol ring (Fig. 5D).

Parent Species	Radical Cation	Neutral Radicals					
		α–H	α–OH	β-H	γ-H	γ-OH	4-OH
V-O-4	116.5 (-5.0)	86.2 (-3.7)	101.1	102.5	105.6	104.6	-
S-O-4	111.4 (-4.8)	84.1 (-3.7)	100.4	98.8	104.1	101.6	73.4 (-3.2)
G-O-4	114.7 (-5.0)	83.4 (-3.6)	101.1	101.3	104.3	102.4	77.8 (-3.4)

Table S3 – Free energies of formation in aqueous solution (kcal mol^{-1}) of various lignin dimer substrate species from their neutral, closed shell parents. Each neutral radical result includes the solvated energy of the removed proton. Corresponding values of the reduction potential for species of interest are given in parentheses (in Volts).

As a result of the enzyme reacting with a substrate molecule, it must either produce the radical cation, or must remove a proton simultaneously with the electron to form the neutral radical. The radical cation is formed by removal of a single electron.

$$S^{\cdot+} + \mathrm{e}^- \rightarrow S \; (E_0 = 5.1, 4.8, 5.0)$$

The potentials for each substrate are given in the order *V*-O-4, *S*-O-4, *G*-O-4 throughout. For the case of formation of neutral radical the deprotonation position must be considered (positions α–H and 4-OH).

$$S^{\cdot}{}_{\alpha-\mathrm{H}} + \mathrm{e}^- + H^+ \rightarrow S \; (E_0 = \; 3.7, 3.7, 3.6)$$

$$S^{\cdot}{}_{4-\mathrm{OH}} + \mathrm{e}^- + H^+ \rightarrow S \; (E_0 = \; 3.2, 3.4)$$

Removal of the 4-OH proton is possible for the phenolic dimers. The potential for removal of this specific proton is lower in both phenolic species than that observed for removal of an α–H proton, meaning that this species will form more readily from both phenolic substrates. The consequent chemistry of the radical lignin dimers is thus determined by the neutral radical formed by deprotonation of the hydroxyl group at position 4.

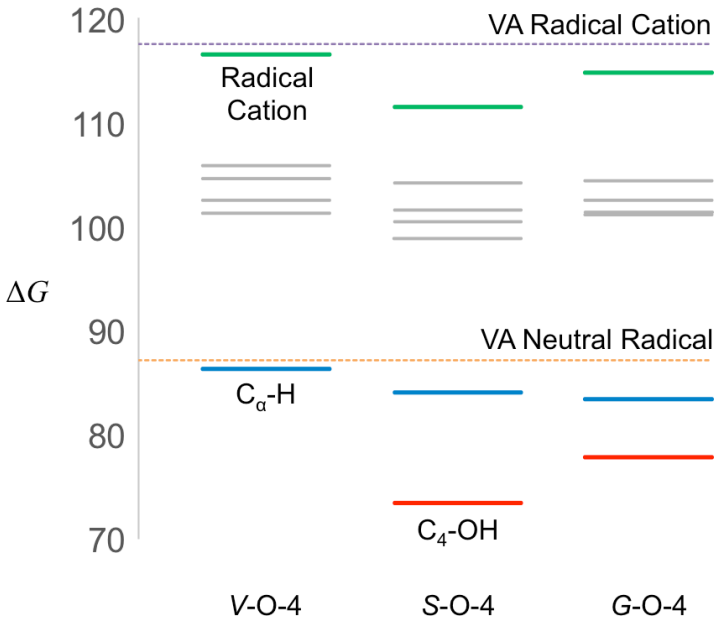

Figure S8 - Graphical presentation of the free energy of formation data. γ-OH, γ-H, α–OH and β-H are shown in gray, the radical cation is in green, α–H in blue and 4-OH in red. All values are in kcal mol^{-1} and are referred to the appropriate closed-shell, neutral substrate species. Dotted lines mark the free energy of formation of the VA radical cation (upper, purple) and neutral radical (lower, orange).

The fact that the enzyme is unable to degrade the non-phenolic dimer indicates that the oxidation potential of the enzyme must be less than 3.7 Volts, as otherwise the enzyme would be able to remove a proton at the α–H position of the *V*-O-4 dimer. However, the experimental results suggest that VP_*Bad* is able to oxidize VA. If this is by the same mechanism as oxidation of the lignin dimers, there is a problem as the results of the calculations suggest that this oxidation requires a slightly higher potential (3.8 V) to achieve than creation of the C_α-deprotonated *V*-O-4 neutral radical (3.7 V). The apparent conflict could be due to oxidation of VA by a different mechanism, as noted above. Indeed, experiments (Fig. S2) show that oxidation of VA can occur by an H_2O_2-independent mechanism (ether an unknown VP_*Bad* functionality or via LiP impurities). Alternatively, the apparent discrepancy could be due to small errors or approximations (e.g. the basis set, particular form of the DFT functional, neglect of solute entropy in the solvation calculations) involved in the theoretical methods. The main point is that the calculations indicate very similar values for the oxidation potential of the neutral VA and *V*-O-4 radicals. Thus the conclusion that the enzyme's tryptophan site either has an oxidation potential similar in magnitude to both ($E_0 \cong 3.7$), or it lies in the range $3.4 \leq E_0 < 3.7$, is justified. The Trp site could *potentially* work via one of two pathways.

$$\mathrm{Trp}^{\cdot+} + \mathrm{e}^- \rightarrow \mathrm{Trp}$$

This would require that the enzyme exist as a radical cation when active (i.e. the proton at the nitrogen atom is maintained) and would produce radical cations from substrates. As Fig. S7 makes clear, if this were possible and the VA radical cation was consequently formed, VP_*Bad* would be able to degrade all three of

the dimers tested in this work by formation of their radical cations. Therefore the 2nd option, where a neutral protein radical is formed in the enzyme redox cycle (as shown by experiment), must be correct.

$$\mathrm{Trp}^{\cdot} + \mathrm{e}^{-} + \mathrm{H}^{+} \rightarrow \mathrm{Trp}\ (3.4 \leq E_0 < 3.7)$$

3 - Depolymerization and Repolymerization of the Substrate

The preceding arguments ultimately result in the presence in solution of radical forms of the *V*-O-4 and *G*-O-4 substrate molecules, which are neutral radicals created by deprotonation of the hydroxyl at the 4 position. It remains to explain why the particular observed products are obtained from these species.

Experiment shows that the *S*-O-4 dimer depolymerizes (Fig. 5E), and the observed products require cleavage of the bond between glycerol C_α and C_1 of the phenol ring). The energy calculations suggest that removal of the 4-OH proton is feasible, and a pathway from the corresponding neutral substrate radical to the observed breakdown products can be suggested, either by the action of a second radical species or possibly by homolysis. Spin density calculations (Fig. 5D) show that the majority of the spin density is present on the phenolic oxygen atom and the carbon atoms *ortho* (C_3, C_5) and *para* (C_1) to it. The presence of a methoxy group at the ortho positions precludes polymerization of the *S*-O-4 dimer, perhaps by restricting the inter-unit C-C distance in solution (which must become short for polymerization to occur) to large values through short-range repulsive forces.

The *G*-O-4 dimer is observed experimentally to polymerize in the presence of the enzyme (Fig. 3). In order for this to be possible, a potential site for bond formation must be present in the substrate. Spin density calculations indicate a greater spin density at the C_5 position for this dimer than for *S*-O-4, along with a reduced spin density at the carbon (C_3) from which cleavage can occur. It is inferred from this result that the polymerization occurs at the 5 position (i.e. *ortho* to the phenol group), which agrees with the experimental observations. The atomic values are shown in Fig. 5D.

Conclusions

Calculations indicate that half-reactions that form neutral radical products have less positive free energies of reaction than those that form radical cations. The lowest free energy pathway to formation of neutral radicals is through removal of the 4-OH proton, whereas removal of the α–H proton requires substantially greater free energy. This explains the experimental observation that phenolic lignin structures are more readily oxidized than non-phenolic structures. The reported calculations suggest that oxidation of VA to the neutral radical will involve a comparable free energy change to that of oxidation of α–H proton in the nonphenolic dimer. This is consistent with prior reports of the use of VA as a mediator to oxidize nonphenolic lignin. Spin density calculations suggest that polymerization of *G*-O-4 occurs at the 5 position, and that this pathway is not favorable for the *S*-O-4 dimer due to the presence of a methoxy group at this position. This explains the experimental observation of polymerization for *G*-O-4 and depolymerization for *S*-O-4.

While useful information has been gained in this study, further improvements are possible. In particular, a full simulation study of the reactions would allow free energy barriers (and thus kinetic effects) to be determined. A more detailed understanding of the processes carried out by the enzyme would allow for a more focused study of the exact steps occurring in the experimental system, allowing further confirmation of conclusions drawn from this work.

References:

1. M. Pérez-Boada, F. J. Ruiz-Dueñas, R. Pogni, R. Basosi, T. Choinowski, M. J. Martínez, K. Piontek and A. T. Martínez, *Journal of Molecular Biology*, 2005, **354**, 385-402.
2. R. Pogni, M. C. Baratto, S. Giansanti, C. Teutloff, J. Verdin, B. Valderrama, F. Lendzian, W. Lubitz, R. Vazquez-Duhalt and R. Basosi, *Biochemistry*, 2005, **44**, 4267-4274.
3. R. Pogni, M. C. Baratto, C. Teutloff, S. Giansanti, F. J. Ruiz-Dueñas, T. Choinowski, K. Piontek, A. T. Martínez, F. Lendzian and R. Basosi, *Journal of Biological Chemistry*, 2006, **281**, 9517-9526.